Available online at www.sciencedirect.com
SCIENCE DIRECT®
Engineering Structures 26 (2004) 693–706
ENGINEERING STRUCTURES
www.elsevier.com/locate/engstruct

Behavior and design of structures with buckling-restrained braces

Jinkoo Kim *, Hyunhoon Choi

Department of Architectural Engineering, Sungkyunkwan University, Chunchun-dong, Jangan-gu, 440-746 Suwon, South Korea

Received 16 May 2003; received in revised form 18 September 2003; accepted 19 September 2003

Abstract

Energy dissipation capacity and earthquake response of steel structures installed with buckling-restrained braces (BRB) were investigated, and a straightforward design procedure to meet a given target displacement was developed. A formulation for optimum yield strength of BRB that maximize the equivalent damping ratio was derived, and nonlinear dynamic time-history analyses were carried out to investigate the seismic response of model structures with BRB. The analysis results show that the maximum displacements of structures generally decrease as the stiffness of the brace increases, and that the maximum displacement of the model structures designed in accordance with the proposed method corresponds well with the given target displacement.

Keywords: Buckling-restrained brace; Equivalent damping; Seismic design; Capacity spectrum method

1. Introduction

The energy dissipation or damage prevention capacity of a steel moment frame can be greatly enhanced by employing buckling-restrained braces (BRB). They usually consist of a steel core undergoing significant inelastic deformation when subjected to strong earthquake loads and a casing for restraining global and local buckling of the core element. According to previous research, a BRB exhibits a stable hysteretic behavior with superb energy dissipation capacity. Watanabe et al. [1] showed the effectiveness of BRB and investigated the effect of outer tube configuration on overall load capacity of the brace. Tremblay et al. [2] conducted a quasi-static loading test on BRB and showed that the strain hardening behavior is most likely the result of Poisson's effects on the steel plate undergoing large inelastic deformation. Huang et al. [3] carried out static and dynamic loading tests on structures with BRB and showed that the energy dissipation capacity of a frame increased with the installation of BRB, and that the main frame remained elastic even when it was subjected to large earthquake load. Black et al. [4] carried out stability analysis against flexural and torsional buckling of BRB, and presented test results of five BRB with various configurations. Their study concluded that BRB is a reliable and practical alternative to conventional lateral load resisting systems.

Inoue and Kuwahara [5] analytically derived the optimum strength of hysteretic dampers assuming that strength and stiffness of the device are independent. Clark et al. [6] proposed a design procedure for structures with BRB, and concluded that frames designed to incorporate BRB following the 1994 Uniform Building Code should use forces compatible with those used for eccentric braced frames rather than those used for special concentrically braced frames, because BRB do not exhibit the stiffness and strength deterioration.

In this study, the energy dissipation capacity and earthquake response of steel structures installed with BRB were investigated. Parametric study was performed for two important design parameters; cross-sectional area and the yield strength of BRB. Based on the results of parametric study, a straightforward design procedure to achieve a target displacement was

* Corresponding author. Tel.: +82-331-290-7563; fax: +82-31-290-7570.
E-mail address: jinkoo@skku.ac.kr (J. Kim).

0141-0296/$ - see front matter © 2003 Published by Elsevier Ltd.
doi:10.1016/j.engstruct.2003.09.010

developed in the framework of the capacity spectrum method. Nonlinear static and dynamic time-history analyses were carried out to investigate the seismic response of model structures with BRB.

2. Equivalent damping of a structure with buckling-restrained braces

Fig. 1 depicts schematically the load–displacement relationship of a structure with BRB. The overall stiffness of the system results from the combination of the stiffness of the main frame and the brace, and the yield points of the combined structure, F_{y1} and F_{y2}, can be obtained as follows

$$F_{y1} = F_{by} + K_s u_{by} \tag{1}$$

$$F_{y2} = F_{by}\left(1 + \beta\frac{u_{sy}}{u_{by}} - \beta\right) + F_{sy} \tag{2}$$

where F_{sy}, u_{sy}, and K_s are the yield force, yield displacement, and lateral stiffness of the main frame, respectively, F_{by} and u_{by} are those of the BRB, respectively, and β is the post-yield stiffness ratio of BRB. The stiffness ratio, S_r, is defined as follows:

$$S_r = \frac{K'_b}{K_s} \tag{3}$$

where K'_b is the lateral stiffness of BRB, which is obtained as follows

$$K'_b = K_b\cos^2\theta = \frac{A_b E_b}{L_b}\cos^2\theta \tag{4}$$

where K_b, A_b, and E_b are the axial stiffness, sectional area, and the elastic modulus of BRB, respectively, L_b is the length of BRB, and θ is the slope of the brace. Alternatively, for the given story stiffness and stiffness ratio, the required cross-sectional area of BRB can be obtained as

$$A_b = \frac{K_b L_b}{E_b} = \frac{K'_b L_b}{E_b\cos^2\theta} = \frac{(S_r K_s)L_b}{E_b\cos^2\theta} \tag{5}$$

Furthermore, the yield strength (F_{by}) and the yield displacement (u_{by}) of the brace can be expressed as follows

$$F_{by} = \frac{(S_r K_s)L_b}{E_b\cos\theta}\sigma_{by} \tag{6}$$

$$u_{by} = \frac{F_{by}}{K'_b} = \frac{L_b}{E_b\cos\theta}\sigma_{by} \tag{7}$$

If the ratio of the yield strength of BRB and the whole system is represented by γ, it can be expressed as follows

$$\gamma = \frac{F_{by}}{F_{y2}} = \frac{F_{by}}{F_{sy} + F_{by}\left(1 + \beta\frac{u_{sy}}{u_{by}} - \beta\right)} \tag{8}$$

When the structural properties remain constant, the yield strength ratio is generally determined by the size and yield stress as well as the post-yield stiffness of BRB. The yield strength of BRB and the structure, F_{by} and F_{sy}, respectively, and the maximum strength of BRB and the structure at the maximum displacement, F_{bm} and F_{sm}, respectively, can be expressed using the strength ratio as follows

$$\begin{aligned}
F_{by} &= \gamma F_{y2}\\
F_{sy} &= \left\{1 - \gamma\left(1 + \beta\frac{u_{sy}}{u_{by}} - \beta\right)\right\}F_{y2}\\
F_{bm} &= F_{by}(1 + \beta\mu_b - \beta) = \gamma(1 + \beta\mu_b - \beta)F_{y2}\\
F_{sm} &= F_{sy}(1 + \alpha\mu_s - \alpha)\\
&= \left\{1 - \gamma\left(1 + \beta\frac{u_{sy}}{u_{by}} - \beta\right)\right\}(1 + \alpha\mu_s - \alpha)F_{y2}
\end{aligned} \tag{9}$$

where α and β are the post-yield stiffness ratio of the structure and the BRB, respectively, $\mu_s = u_m/u_{sy}$ and $\mu_b = u_m/u_{by}$. It is generally required that BRB should start yielding before the main frame does to minimize the earthquake-induced damage in the structural members; i.e., the yield displacement of the BRB should be less than that of the frame.

Referring to Fig. 2, the equivalent viscous damping ratio of the system under steady-state harmonic load

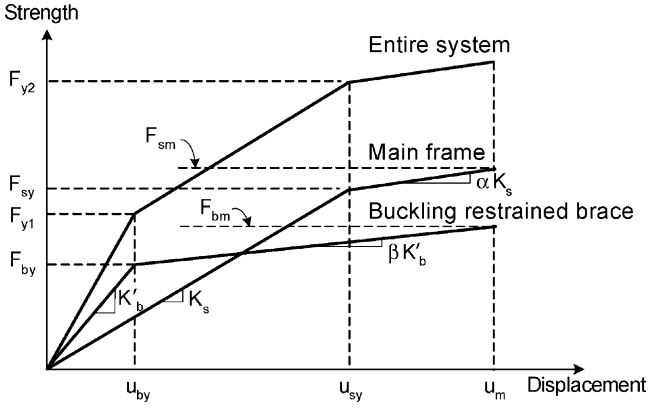

Fig. 1. Load–displacement relationship of a structure with BRB.

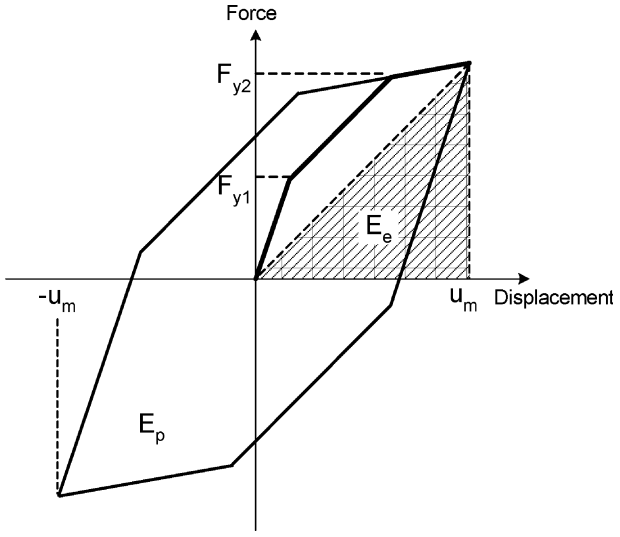

Fig. 2. Hysteresis loop of a structure with BRB.

can be defined as follows:

$$\zeta_{eq} = \frac{E_p}{4\pi E_e} \tag{10}$$

where E_p is the dissipated energy of the system per cycle, which is equivalent to the area enclosed by the hysteresis loop, and E_e is the stored strain energy, which corresponds to the area of the hatched triangle in the figure. The dissipated and stored energy are composed of two components, components contributed from the main frame, E_{ps} and E_{es}, and from the devices, E_{pb} and E_{eb}:

$$4\pi\zeta_{eq} = \frac{(E_{pb} + E_{ps})}{(E_{eb} + E_{es})} \tag{11}$$

The above equation can be rewritten as follows by substituting appropriate expressions for the stored and dissipated energy:

$$\zeta_{eq} = \frac{1}{4\pi}\frac{4\{F_{sy}u_m - u_{sy}F_{sy}(1+\alpha\mu_s-\alpha)\} + 4\{F_{by}u_m - u_{by}F_{by}(1+\beta\mu_b-\beta)\}}{\frac{1}{2}u_m\{F_{by}(1+\beta\mu_b-\beta) + F_{sy}(1+\alpha\mu_s-\alpha)\}} \tag{12}$$

The definitions for variables used can be found in Fig. 1. The above expression for equivalent damping can be rewritten using the stiffness ratio S_r and the strength ratio γ as follows

$$\frac{\pi}{2}\xi_{eq} = 1 + \frac{\beta\{\gamma(S_r+1) - S_r\}}{1+S_r\beta} - \frac{1+\alpha\mu_s-\alpha}{\mu_s}\left(\frac{1-\gamma+\beta\gamma}{1+S_r\beta}\right) + \frac{\gamma^2(1+S_r\beta)}{S_r\mu_s(1-\gamma+\gamma\beta)}(\beta-1) - \beta\gamma \tag{13}$$

The strength ratio γ can be independent of the stiffness ratio S_r if the size of BRB remains constant and only the yield stress of BRB changes. In this case, the optimum yield strength ratio γ_{opt} that maximizes the equivalent damping can be obtained by equating the derivative of the above expression with respect to γ with zero, i.e., $\partial((\pi/2)\zeta_{eq})/\partial\gamma = 0$; as was done by Inoue and Kuwahara [5] for elastic-perfectly plastic hysteretic dampers:

$$\gamma_{opt} = \frac{1}{1-\beta} \times \left\{1 - \frac{1+S_r\beta}{\sqrt{(1+S_r\beta)^2 - S_r(\beta\mu_s S_r + 1 + \alpha\mu_s - \alpha)(\beta-1)}}\right\} \tag{14}$$

It would be more useful to transform the above expression to the optimum yield stress of BRB using Eq. (8):

$$\sigma_{by,opt} = \frac{\gamma_{opt}F_{sy}(1+S_r\beta)}{A_b\cos\theta(1-\gamma_{opt}+\gamma_{opt}\beta)} \tag{15}$$

This equation corresponds to the optimum yield stress of BRB which maximizes the equivalent damping of the system.

3. Parametric study for equivalent damping

The equivalent damping, expressed in Eq. (13), is plotted in Fig. 3 for variables such as strength ratio, stiffness ratio, yield stress of BRB, initial to post-yield strength ratio, and ductility ratio. The yield strength and the initial stiffness of the model structure are set to be 240 MPa and 44 kN/m, respectively. It can be seen in Fig. 3(a) that the equivalent damping is maximized at a specific yield stress of BRB. However, in practical range of yield stress for BRB, say from 100 to 330 MPa, the equivalent damping generally increases as the yield stress increases. In this region, it is also increasing function of stiffness ratio and the ductility demand. It can also be noticed that as the ductility demand increases the equivalent damping also increases. Fig. 3(b) plots the equivalent damping ratio vs. stiffness ratio when $\alpha = 0.1$ and $\beta = 0.05$. It can be observed that

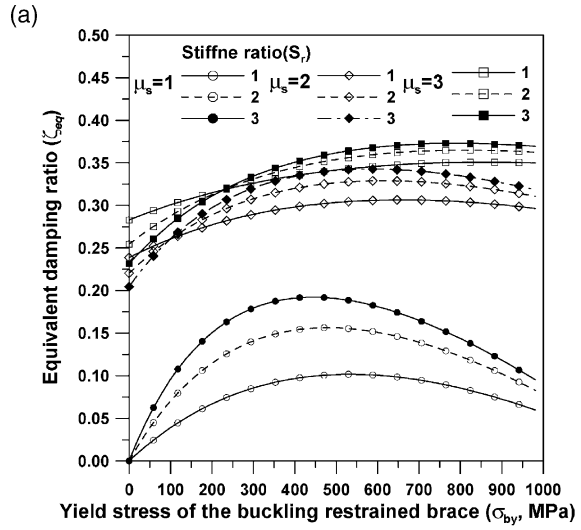

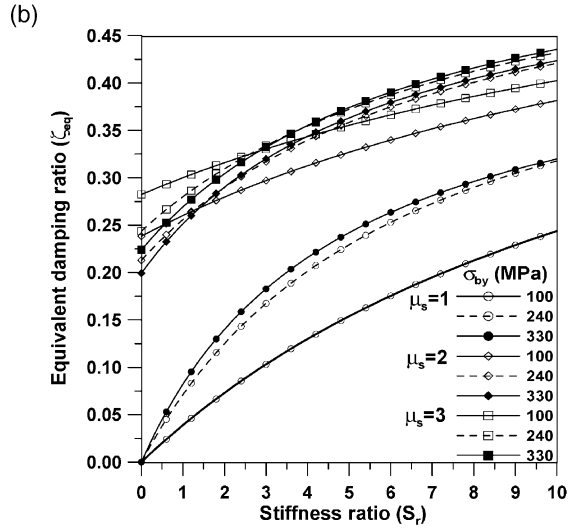

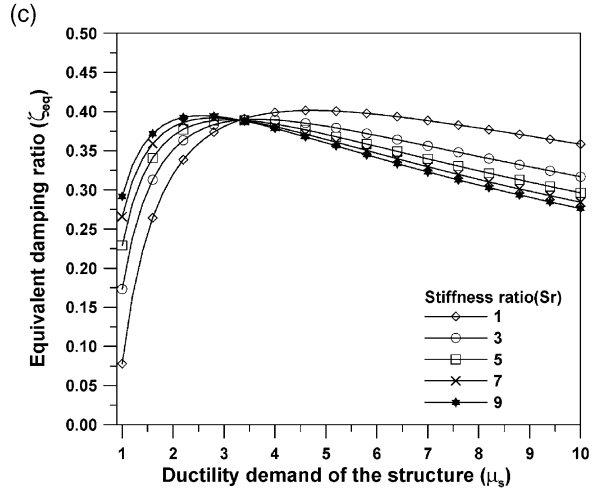

Fig. 3. Equivalent damping ratio of a SDOF structure with BRB. (a) Equivalent damping vs. yield stress of BRB ($\alpha = 0.1$ and $\beta = 0.05$). (b) Equivalent damping ratio vs. stiffness ratio ($\alpha = 0.1$, $\beta = 0.05$). (c) Equivalent damping ratio vs. ductility demand for various stiffness ratio.

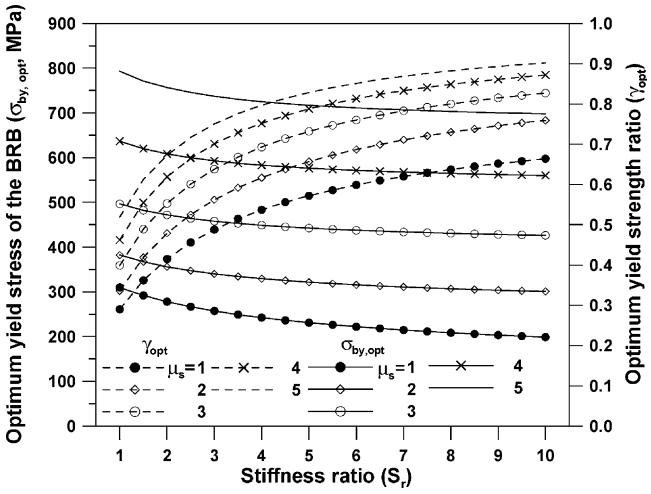

Fig. 4. Optimum yield stress of BRB and optimum yield strength ratio for various stiffness ratios.

the equivalent damping is monotonically increasing function of the stiffness ratio. These observations lead to the conclusion that BRB with larger sectional area always results in higher equivalent damping. It should be noted, however, that although the equivalent damping increases as the size of BRB increases, the earthquake-induced dynamic motion may also increase as a result of reduced elastic period. Fig. 3(c) plots the equivalent damping ratio vs. ductility demand for various stiffness ratios. It can be observed that up to the ductility demand of approximately 3, the equivalent damping increases as the stiffness ratio and the ductility demand increase. This trend is reversed as the ductility demand increases more than 3. These observations imply that BRB with larger cross-sectional area results in higher equivalent damping when the structure undergoes small lateral displacement, and that the opposite is true at larger displacement.

Fig. 4 presents the optimum yield stress of BRB and the strength ratio at the optimum yield stress with respect to the stiffness ratio, which shows that the optimum yield stress decreases and the optimum strength ratio increases as the stiffness of BRB increases. This means that as larger size of BRB is used, steel with lower yield stress needs to be used in BRB for maximizing equivalent damping.

4. Seismic response of structures with BRB

4.1. Model structures and earthquake loads

The 5- and 10-story structures shown in Fig. 5 were used to investigate the seismic response of structures with BRB. They were designed for gravity and wind loads to simulate the structures constructed before the Korean seismic design code [7] were enforced in 1988.

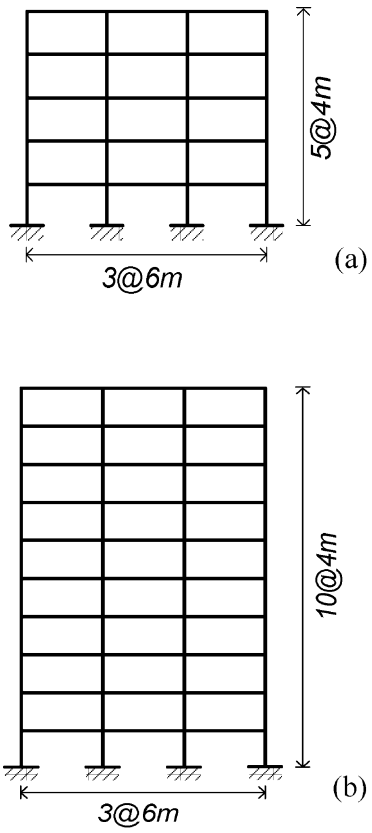

Fig. 5. Model structures for analysis. (a) Five-story structure. (b) Ten-story structure.

Dead load of 54 MPa and live load of 25 MPa were applied throughout the stories, and the wind load with the basic wind speed of 30 m/s at the height of 10 m from the ground level was used for lateral load. The yield stress of the structural steel is 240 and 330 MPa for beams and columns, respectively. The elastic modulus of the structure was modified so that the fundamental natural periods become close to those provided by the code formula. The member selection was carried out using the program code MIDAS-GEN [8], which is a three-dimensional analysis and design program with powerful pre- and post-processors, and the selected cross-sectional dimensions of the structural members are listed in Table 1. The fundamental natural periods of the 5- and 10-story structures computed from eigenvalue analysis turned out to be 1.37 and 2.28 s, respectively. These are too large for natural period of real building structures with similar heights. These unrealistic natural periods result from two-dimensional modeling of structures. Therefore to simulate the dynamic behavior of realistic structures, the elastic modulus was modified so that the natural periods of the model structures coincide with those obtained from code formula. Even though this will result in reduced lateral displacement, the general conclusion of this study will not be affected by the modification of the elastic modulus. Table 2 presents the story stiffness, inter-story drift ratio and story shear force ratio of the model structures obtained from pushover analysis.

Nonlinear time-history analysis was carried out using El Centro and Mexico earthquake records scaled to effective peak acceleration (EPA) of 0.4 g. It was assumed that the structural members show bi-linear force–deformation relationship with post-yield stiff-

Table 2
Story stiffness, inter-story drift ratio and story shear force ratio of the model structures obtained from pushover analysis

Story	Story stiffness (kN/cm)	Inter-story drift ratio	Story shear force ratio
(a) *5-Story structure*			
1	276.7	0.849	1.000
2	145.4	1.000	0.947
3	125.9	0.924	0.810
4	122.1	0.691	0.593
5	114.6	0.434	0.314
(b) *10-Story structure*			
1	578.3	0.809	1.000
2	328.1	0.946	0.988
3	277.4	1.000	0.957
4	250.1	0.992	0.905
5	213.8	0.941	0.833
6	205.2	0.805	0.738
7	202.8	0.602	0.622
8	197.0	0.416	0.488
9	174.7	0.224	0.337
10	158.5	0.116	0.172

Table 1
Sectional properties of model structures (unit: mm)

Model	Levels	Columns		Beams
		Interior columns	Exterior columns	
5-story	3–5	H344 × 354 × 16 × 16	H298 × 299 × 9 × 14	H350 × 175 × 7 × 11
	1–2	H350 × 350 × 12 × 19	H300 × 300 × 10 × 15	H350 × 175 × 7 × 11
10-story	8–10	H344 × 354 × 16 × 16	H298 × 299 × 9 × 14	H350 × 175 × 7 × 11
	5–7	H350 × 350 × 12 × 19	H300 × 300 × 10 × 15	H396 × 199 × 7 × 11
	1–4	H400 × 400 × 13 × 21	H344 × 348 × 10 × 16	H400 × 200 × 8 × 13

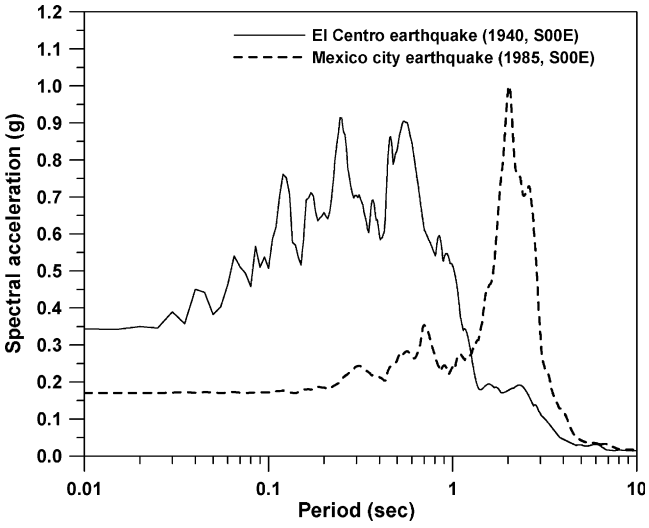

Fig. 6. Response spectra of input earthquake records.

ness ratio of 0.05. The program code DRAIN2D+ [9] was used for nonlinear static and dynamic analysis. Fig. 6 presents the spectral acceleration of the two earthquake records, which shows that the two records have quite different dynamic characteristics.

4.2. Story-wise distribution of brace

The cross-sectional area of BRB corresponding to the story stiffness ratio from 1 to 10 is obtained using Eq. (5). Two types of BRB with yield stress of 100 and 240 MPa were used in the analysis. For story-wise distribution of BRB, the following four methods were applied:

- Case 1: BRB is distributed proportional to story stiffness
- Case 2: BRB with the same size is used in every story
- Case 3: BRB is distributed proportional to the inter-story drift resulting from pushover analysis
- Case 4: BRB is distributed proportional to story shear

The same amount of BRB obtained in Case 1 is used in the other cases for proper comparison of the effectiveness of the distribution methods.

4.3. Maximum roof story displacement of the model structures

Figs. 7 and 8 show the maximum roof displacements of the 5- and 10-story model structures, respectively, subjected to the two earthquake ground excitations. The BRB with yield stress of 100 and 240 MPa were

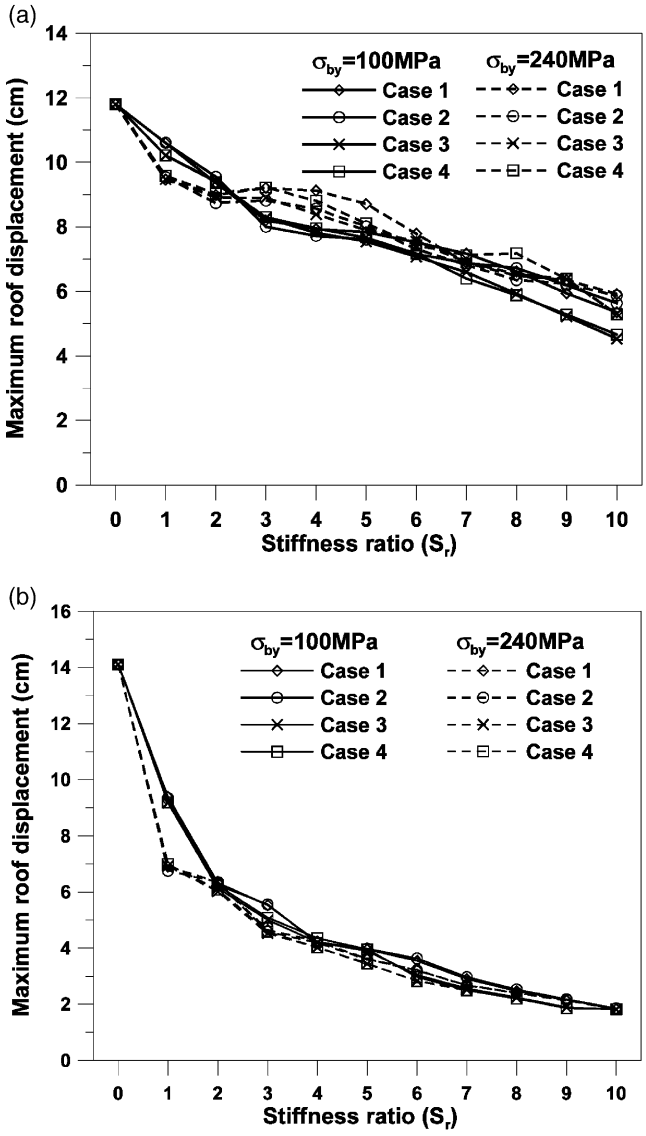

Fig. 7. Maximum top story displacement of the 5-story structure with four different BRB distributions. (a) El Centro earthquake. (b) Mexico earthquake.

installed in the structures by four different story-wise distribution patterns. In Fig. 7, it can be observed that the maximum roof displacement of the 5-story structure generally decreases as the stiffness of BRB increases. It can be seen in Fig. 7(a) that for El Centro earthquake BRB with higher yield stress works better in reducing maximum displacement for smaller BRB ($S_r = 1,2$), whereas BRB with lower yield stress is slightly more effective for larger ones (S_r higher than 3). No distinct trend can be observed for the effectiveness of different story-wise BRB distribution methods. Fig. 8 shows the maximum displacement of the 10-story structure subjected to the two earthquake records, where it can be observed that the maximum

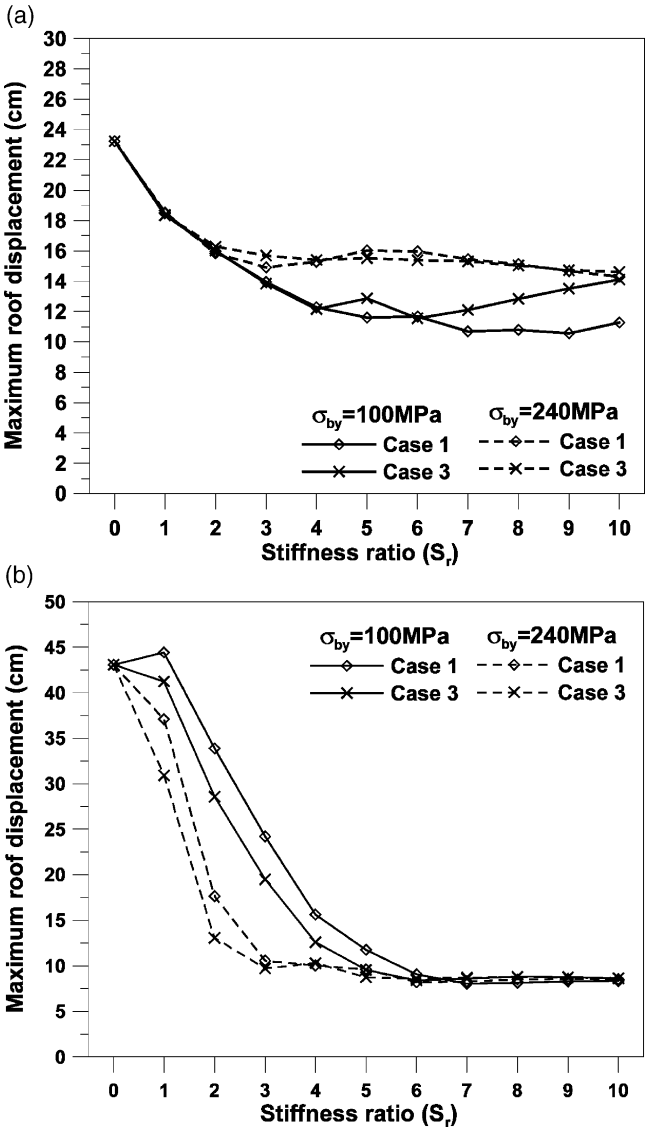

Fig. 8. Maximum top story displacement of the 10-story structure. (a) El Centro earthquake. (b) Mexico earthquake.

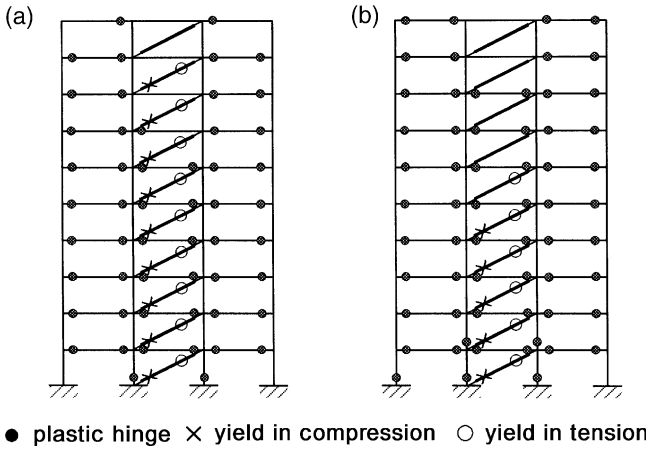

Fig. 9. Location of plastic hinges caused by El Centro earthquake. (a) $\sigma_{by} = 100$ MPa. (b) $\sigma_{by} = 240$ MPa.

displacement decreases as S_r increases, but stops decreasing as the stiffness of BRB increases above a certain value. This phenomenon is due to the magnification of earthquake load in the structure as the stiffness of BRB and consequently the natural frequency of the structure increase. Also, in the 10-story structure, the effectiveness of the BRB's yield stress also varies for different earthquakes.

4.4. Formation of plastic hinges and accumulated plastic deformation

The locations of plastic hinges formed in the 10-story model structures by El Centro earthquake are shown in Fig. 9. Braces with the same size were installed throughout the stories. In both cases, the stiffness ratio, S_r, was set to be 4. It can be seen in the figures that the formation of plastic hinges in BRB highly depends on the yield strength of BRB; when BRB with $\sigma_{by} = 100$ MPa is utilized most BRB yielded, while some BRB with strength $\sigma_{by} = 240$ MPa did not yield even when the beams or columns around them already yielded. This means that when BRB with lower yield strength is used, more vibration energy is dissipated by BRB and less damage occurs in other structural members.

Fig. 10 shows that the accumulated plastic deformation of BRB with $\sigma_{by} = 100$ MPa is much larger than that occurring at BRB with $\sigma_{by} = 240$ MPa, which implies that more vibration energy can be dissipated by plastic deformation of BRB with lower yield strength.

5. Design procedure for BRB

In the previous sections, it was observed that the equivalent damping of a structure with BRB generally increases and the maximum displacement decreases almost monotonically as the stiffness of BRB increases. Although the yield stress of BRB can be another design parameter influencing on structural responses, its importance is limited due to the lack of availability in the industry. Therefore it seems to be rational to take the cross-sectional area of BRB as the primary design variable, and to determine the proper size in such a way that the desired displacement limit state of a structure is satisfied.

In this regard, a straightforward design procedure for BRB to meet a given structural performance point is developed. The maximum roof–story dis-

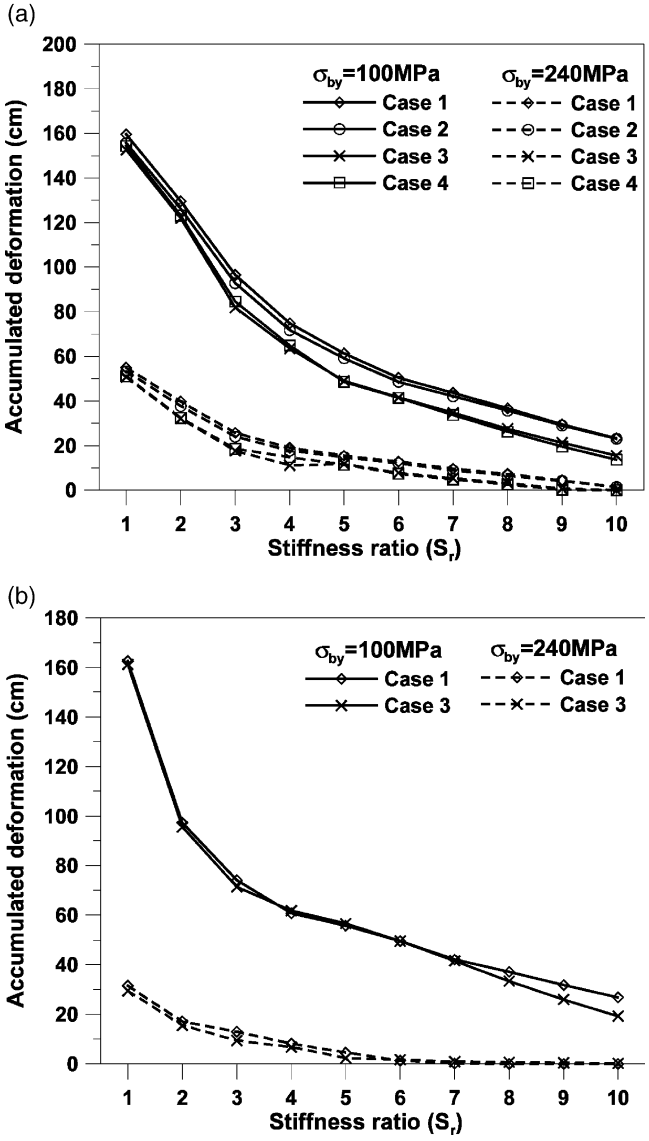

Fig. 10. Accumulated plastic deformation of BRB. (a) Five-story structure. (b) Ten-story structure.

placement is taken as the target performance point. The proposed method is based on a simple modification of the capacity spectrum method (CSM) described in FEMA-273 and 274 [10], where the effective damping of a structure with hysteretic damping device is obtained as a linear combination of: (1) the equivalent damping of the structure, (2) the equivalent damping of the device, and (3) the inherent viscous damping of the structure. In this study, for design purpose, the amount of total effective damping required for a structure to satisfy the given performance point is obtained first, and then the equivalent damping needed to be supplied by the BRB is obtained from the difference between the total demand of damping and the hysteretic damping of the structure at the target displacement plus the inherent damping. The required amount of BRB is computed based on the assumption that the total effective damping is provided by plastic deformation of BRB. The whole process is conveniently carried out by transforming both demand and capacity curves into the so-called acceleration–displacement response spectrum (ADRS) coordinates. The procedure avoids the conventional trial and error process for design of supplemental dampers, and has advantage of using nonlinear static analysis instead of nonlinear dynamic analysis.

5.1. Construction of a capacity–demand diagram

The relationship between the base shear and the top story displacement, which is generally called the pushover curve or capacity curve, is obtained by gradually increasing the lateral seismic story forces appropriately distributed over the stories. In this study, lateral seismic load is applied in proportion to: (i) the fundamental mode shape; (ii) the mode shape combined by square-root of sum of square method (SRSS mode); and to (iii) the equivalent mode shape [11]. The demand curve can be derived from an elastic response spectrum, using a level of viscous damping consistent with the energy dissipated by the building in one cycle of loading as suggested in FEMA-273 [10]. The performance point is obtained from the cross-point of the demand and the capacity curves plotted in the spectral acceleration vs. spectral displacement domain, which is known as the acceleration–displacement response spectra (ADRS).

5.2. Computation of the required equivalent damping

The additional equivalent damping required to be supplied to the structure was computed from the difference between the overall effective damping of the structure to meet the target displacement and the equivalent damping contributed from the hysteretic energy dissipation of the structural members obtained from the capacity spectrum at the target displacement. The proper damper size was computed from the overall equivalent damping required to meet the target. The design process needs iteration because the added brace changes the capacity curve of the structure.

FEMA-274 presents the effective damping of a structure with added hysteretic dampers as follows:

$$\zeta_{\text{eff}} = \zeta_{\text{d}} + \zeta_{\text{s}} + \zeta_{\text{i}} \tag{16}$$

where ζ_d corresponds to the equivalent damping contributed from the hysteretic behavior of the BRB, ζ_s is the equivalent damping contributed from inelastic deformation of the structural members, and ζ_i is the inherent viscous damping of the structure. The equivalent damping of the structure itself at the target performance point, ζ_s, can be expressed as follows referring to Fig. 11:

$$\zeta_s = \frac{2(S_{ay}S_{dt} - S_{dy}S_{at2})}{\pi S_{at2}S_{dt}} \tag{17}$$

where S_{ay} and S_{dy} are the acceleration and the displacement at yield, respectively, S_{at2} and S_{dt} are the acceleration and displacement at the target, respectively.

For determination of proper amount of supplemental dampers to be supplied to meet a given performance objective, it is suggested in this study that Eq. (16) be converted to the following form to obtain the required supplemental damping, ζ_d, for the given total effective damping of the whole system and the equivalent damping of the structure itself:

$$\zeta_d = \zeta'_{eff} - \zeta_s - \zeta_i \tag{18}$$

where ζ'_{eff} is the overall effective damping of the system required to restrain the structure below the target displacement, which corresponds to the damping ratio of the demand curve that intersects the capacity curve at the target displacement on the ADRS. Throughout the study, the inherent viscous damping is assumed to be 5% of the critical damping. In multi-story structures, the process of obtaining the required damping is carried out after they are transformed to equivalent SDOF systems as described in ATC-40 [12].

5.3. Design of BRB to meet a target displacement

Once the equivalent damping required to meet a target displacement is obtained from the equivalent SDOF system, the next step is to determine the size of BRB in each story that can realize the required supplemental damping when they are installed in the original MDOF structure. In this study, it is assumed that single BRB is installed in each story as a diagonal brace, as described in Fig. 12. Using the relationship between the equivalent damping and the dissipated energy (E_{DB}) and the stored energy (E_{SB} and E_{SS}), the cross-sectional area of each brace can be obtained from the following relation for the given damping ratio:

$$\zeta_d = \frac{1}{4\pi}\frac{E_{DB}}{E_{SB}+E_{SS}} = \frac{\frac{\sigma_{by}}{E_b}\sum_j\left(K_b\delta_j\cos\theta_j L_{bj} - \frac{\sigma_{by}L_{bj}^2}{E_b}\right)}{\frac{2\pi^3}{T^2}\sum_j m_j\Delta_j^2 + \frac{\pi\sigma_{by}}{2E_b}\sum_j K_b\delta_j L_{bj}\cos\theta} \tag{19}$$

where Δ_j and δ_j denote the story displacement and the inter-story drift at the jth story, respectively, as denoted in Fig. 12. If the size of the brace is the same throughout the stories, the stiffness of each

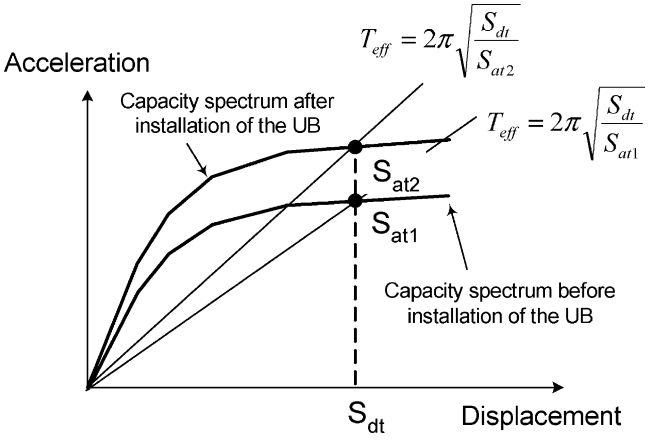

Fig. 11. Capacity curve before and after the installation of BRB.

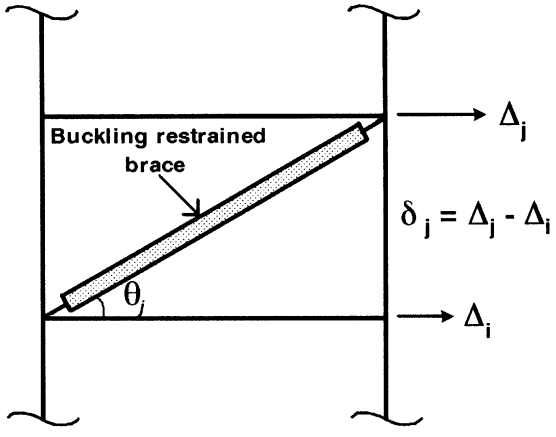

Fig. 12. Notation for story drift of a frame with BRB.

BRB can be obtained as

$$K_b = \frac{\pi\zeta_d \frac{2\pi^2}{T^2}\sum_j m_j\Delta_j^2}{A-B} \tag{20}$$

where

$$A = \frac{\sigma_{by}}{E_b}\sum_j\left(L_{bj}\delta_j\cos\theta_j - L_{bj}^2\frac{\sigma_{by}}{E_b}\right)$$

and

$$B = \frac{\sigma_{by}\pi\beta_d}{2E_b}\sum_j\delta_j\cos\theta_j.$$

The size of the brace obtained in Eq. (20), however, is not the final one because the effect of the brace was not considered in the construction of the capacity curve. Therefore with the first trial value for the size of BRB, new capacity spectra are constructed, and the effective damping of the system and the equivalent damping of the structure are computed again. Then the next trial size of the brace can be computed. The trial values will converge fast after a few iterations.

It should be noted that since the proposed design procedure is derived based on the assumption that all the required equivalent damping is supplied by the plastic deformation of BRB, it may be more accurately applied to structures with BRB made of low-yield strength steel, in which BRB experiences extensive plastic deformation and the plastic deformation of structure itself is minimized.

6. Application of the design procedure

6.1. Model structures and the earthquake design spectrum

In addition to the 5- and 10-story structures presented in Fig. 5, a three-bay 20-story structure with the same story height and span length was prepared for the application of the proposed design procedure. The dynamic modal characteristics of the model structures to be used in the nonlinear static procedure are presented in Table 3. The base shear–top story displacement relationships (pushover curves) were obtained with the lateral story forces gradually increased until the top story displacement reached 4% of the total structure height using DRAIN2D+ [9]. Then these force–displacement curves were transformed into the capacity curves of equivalent SDOF systems (Fig. 13).

For numerical analysis, the Newmark–Hall design spectrum with peak ground acceleration of 0.4 g was used. For time-history analysis, an earthquake time-history was generated using SIMQKE [13] based on the design spectrum. In Fig. 14, the design spectrum is compared with the response spectrum constructed from the earthquake time-history record, where it can be observed that the response spectrum generally fits well with the original design spectrum in period longer than 1.0 s. However, in short-period region, the spectral values of the response spectrum are highly irregular and larger than those of design spectrum. In this study, the response spectrum instead of design spectrum was used in the nonlinear static design procedure so that the time-history analysis results can be compared with the target design value on equal basis.

6.2. Estimation of performance points

The performance points of the model structures were obtained using CSM, and they were transformed to the maximum roof displacements. Then from the pushover analysis to the performance points, the story displacements could be obtained and were plotted in Fig. 15.

Table 3
Dynamic characteristics of the model structures

Model	Modes	1	2	3	4	5
5-Story	Period (s)	0.91	0.28	0.15	0.10	0.08
	Modal participation factor	1.28	0.45	0.25	0.20	0.12
	Effective mass (%)	81.67	10.98	4.46	2.11	0.78
10-Story	Period (s)	1.41	0.49	0.28	0.19	0.14
	Modal participation factor	1.34	0.51	0.30	0.22	0.16
	Effective mass (%)	77.54	11.68	4.28	2.23	1.53
20-Story	Period (s)	3.24	1.12	0.65	0.45	0.34
	Modal participation factor	1.37	0.56	0.32	0.22	0.17
	Effective mass (%)	74.71	13.02	4.24	2.27	1.46

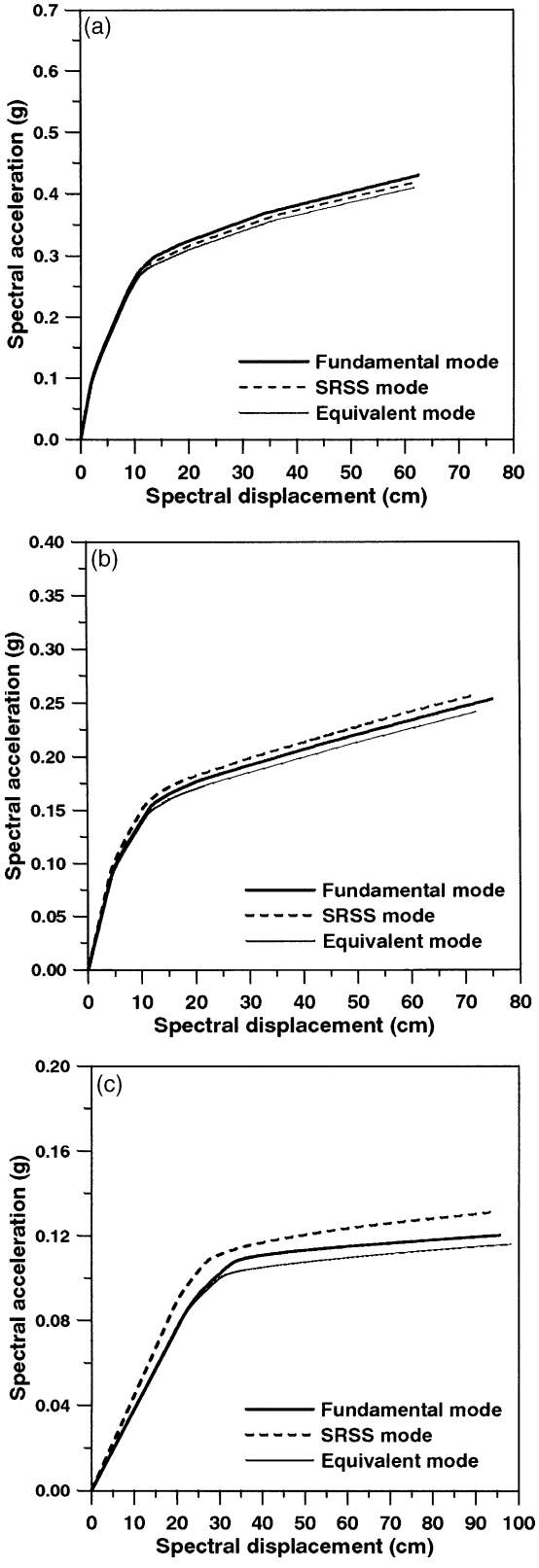

Fig. 13. Capacity curves of model structures for various lateral load configurations. (a) Five-story structure. (b) Ten-story structure. (c) Twenty-story structure.

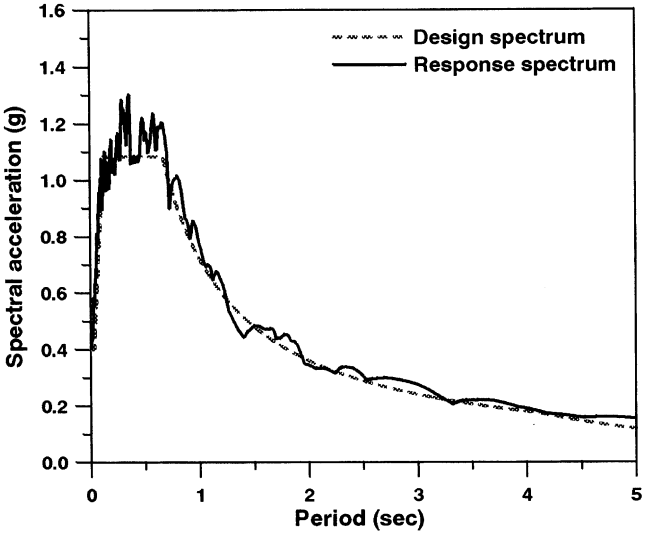

Fig. 14. Newmark–Hall design spectrum and response spectra of artificial earthquake records.

The results from the time-history analysis using DRAIN2D+ were plotted together with the results from CSM using the three different patterns for lateral story forces. It was assumed that point-plastic hinge occurred only at element ends. It can be noticed that the maximum story displacements predicted by CSM are lower than those computed from time-history analysis, although the difference is not significant.

6.3. Design of BRB to meet a target displacement

In this study, the target displacement at the top story of each model structure was arbitrarily set to be 0.5% of the structure height, which is 10, 20 and 40 cm for the 5-, 10- and 20-story model structures, respectively. These correspond to approximately 50%, 20%, and 30% reduction of the maximum displacements, respectively. The 0.5% drift ratio corresponds to the limit state for the 'functional' performance objective recommended by SEAOC Blue Book [14], and the structures behave almost elastically in this limit state. The required supplemental equivalent damping to meet the target displacement was estimated first by the proposed method and was presented in Table 4.

With the required supplemental damping ratios at hand, the next step is to distribute the damping throughout the stories using Eq. (19) or (20), for which the story-wise variation of two categories of variables needs to be assumed in advance: the one is the variation of story displacement and the inter-story drift (Δ_j and δ_j, respectively), and the other is the variation of the BRB's stiffness (cross-sectional area). In this study, two patterns of story displacement are applied: (1) story displacement proportional to the fundamental

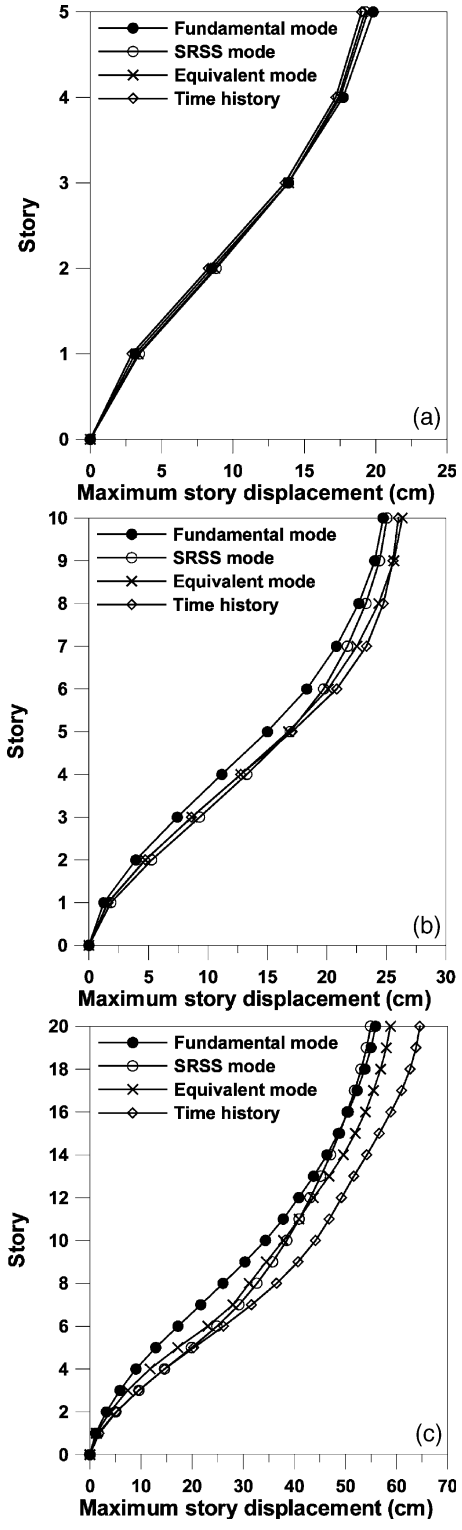

Fig. 15. Maximum story displacements of the model structures. (a) Five-story structure. (b) Ten-story structure. (c) Twenty-story structure.

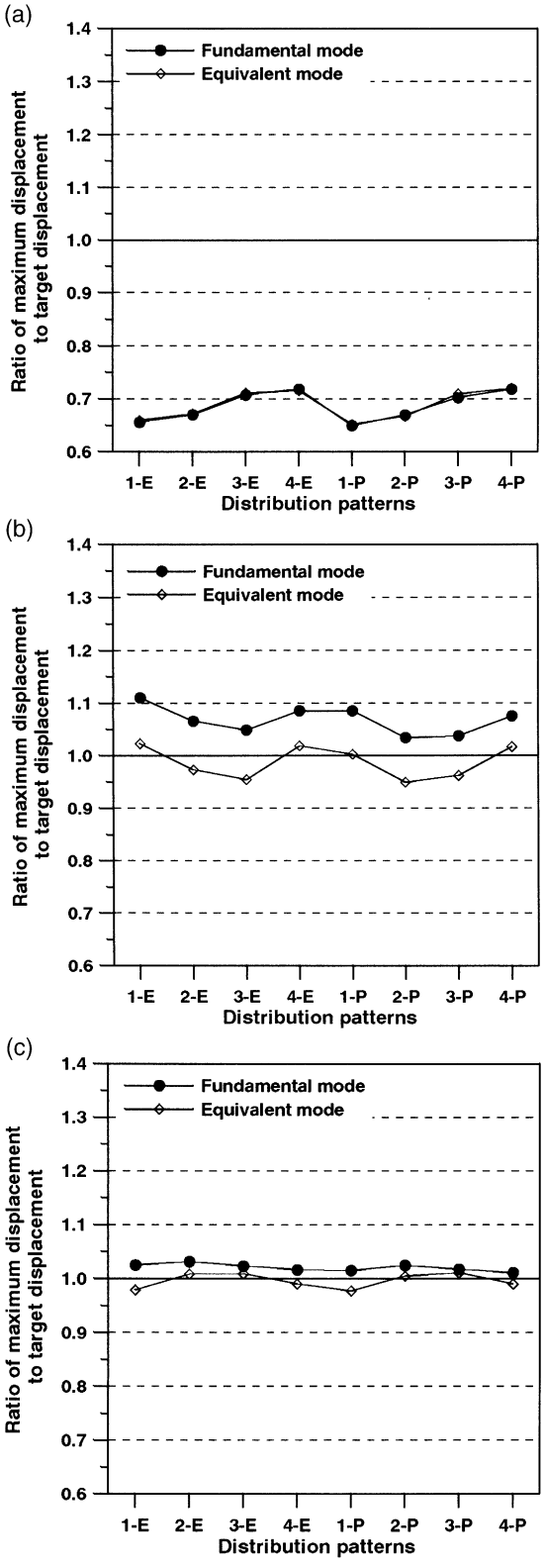

Fig. 16. Ratio of the maximum displacement to target displacement of model structures. (a) Five-story structure. (b) Ten-story structure. (c) Twenty-story structure.

mode shape (denoted by - E), and (2) story displacement proportional to the pushover curve (denoted by - P). Also, for the distribution of the BRB's stiffness,

Table 4
Required equivalent damping to be supplied by BRB (units: cm, g)

Model	Method	Equivalent SDOF system		ζ'_{eff}	ζ_d
		Displacement	Acceleration		
5-Story	1st mode	7.802	0.348	0.292	0.243
	Equivalent mode	7.709	0.348	0.291	0.242
10-Story	1st mode	14.960	0.208	0.286	0.109
	Equivalent mode	14.403	0.213	0.290	0.138
20-Story	1st mode	29.112	0.144	0.218	0.168
	Equivalent mode	27.624	0.138	0.239	0.189

the previous four distribution cases were utilized (see Section 4.2).

6.4. Comparison with time-history analysis

Time-history analyses were conducted for the model structures reinforced with BRB, and the ratios of the maximum displacements to target displacements were plotted in Fig. 16. It can be observed that the maximum displacements of the 10- and 20-story structures retrofitted by the proposed method coincide well with the target displacements. However, those of 5-story structure underestimate the target displacement as much as 25–35% depending on the story-wise distribution methods of BRB. The discrepancy results from the fact that the response spectrum is highly irregular in the region of short natural period, which causes inaccuracy in the process of CSM. It can also be noticed that the story force distribution based on the equivalent mode results in the maximum displacements closer to the target.

Fig. 17 presents the total sectional area of BRB installed in the model structures by the different distribution methods. In the 5-story structure, the difference between the required amounts of BRB determined by the different story force distribution methods is negligible. However, in the taller structures, the use of the equivalent mode results in larger amount of BRB to achieve the same target displacement. This result could be predicted from observing in Table 4 that the required amount of equivalent damping is larger for those cases. In all structures, the required areas for the Cases 3 and 4, stiffness distribution methods are lower than those for the other cases.

7. Conclusions

This study investigated the equivalent damping and performance of structures with BRB, and presented a design procedure to meet a given target displacement in the framework of the capacity spectrum method. The conclusions drawn from the presented study are summarized as follows:

1. The equivalent damping ratios of SDOF structures with BRB generally increase as the stiffness of BRB increases. There exist points of optimum yield stress of BRB which maximizes the equivalent damping. The optimum yield stress decreases as the stiffness of BRB increases and as the ductility demand decreases.
2. The maximum displacements of structures generally decrease as the stiffness of BRB increases.
3. The use of low strength steel for BRB, which undergoes larger plastic deformation and dissipates more energy, is beneficial for reducing structural damage.
4. Story-wise distribution of BRB in proportion to the story drifts and story shears resulted in better structural performance.
5. The maximum displacements of the model structures, designed in accordance with the proposed method, corresponds well with the given target displacements.

There are two independent design parameters for BRB: stiffness and strength. According to the analysis results, there exists a point of optimal yield stress that maximize the equivalent damping ratio of the structure. However, the yield stress of steel that is available in the market is in discrete values. Also, the analysis results show that structural responses do not change monotonically as the yield stress of BRB increases or decreases. Therefore the most probable option that a structural engineer can take is to control stiffness by varying cross-sectional area. As the maximum displacement of model structures generally decreases monotonically as the stiffness of BRB increases, the stiffness of BRB can be a useful design parameter for seismic design.

Acknowledgements

This research is funded by the Korea Science and Engineering Foundation under Grant No R01-2002-000-00025-0. This financial support is gratefully acknowledged.

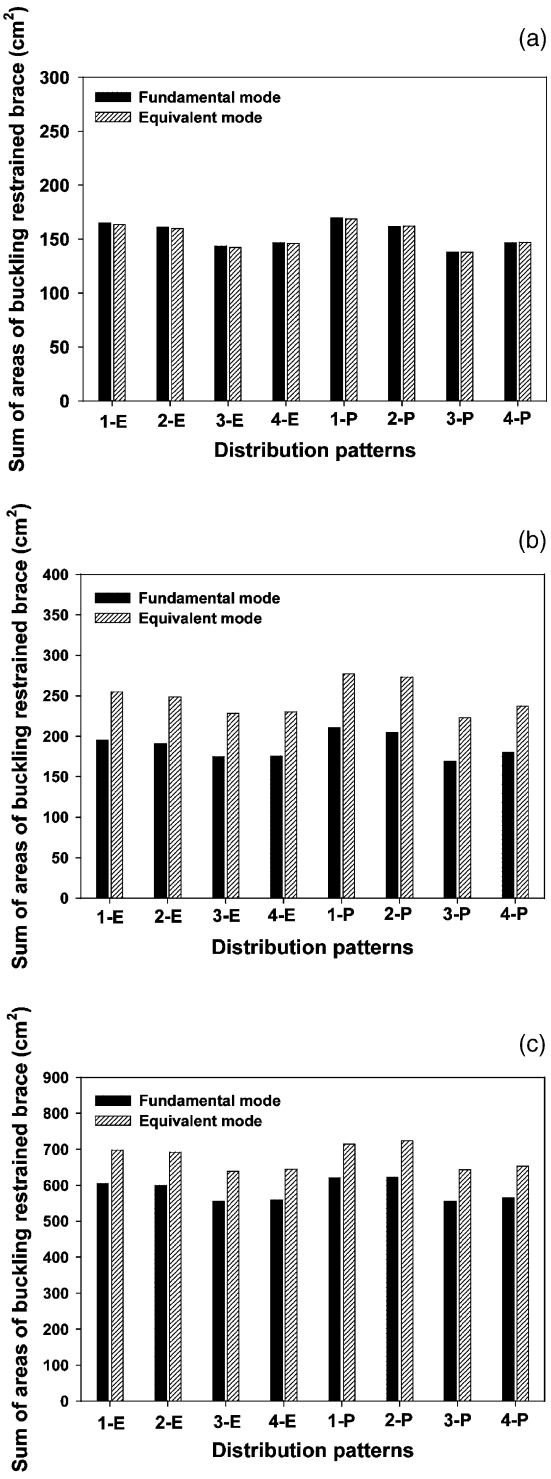

Fig. 17. Summation of required cross-sectional area of BRB. (a) Five-story structure. (b) Ten-story structure. (c) Twenty-story structure.

References

[1] Watanabe A, Hitomoi Y, Saeki E, Wada A, Fujimoto M. Properties of braces encased in buckling–restraining concrete and steel tube. In: Proceedings of 10th World Conference on Earthquake Engineering. Tokyo–Kyoto, Japan. 1988.

[2] Tremblay R, Degrange D, Blouin J. Seismic rehabilitation of a four-story building with a stiffened bracing system. In: Proceeding of the 8th Canadian Conference on Earthquake Engineering. Vancouver; 1999.

[3] Huang YH, Wada A, Sugihara H, Narikawa M, Takeuchi T, Iwata M. Seismic performance of moment resistant steel frame with hysteretic damper. The 3rd International Conference STESSA, Montreal, Canada; 2000.

[4] Black C, Makris N, Aiken I. Component testing, stability analysis and characterization of buckling restrained braces. Final Report to Nippon Steel Corporation, 2001.

[5] Inoue K, Kuwahara S. Optimum strength ratio of hysteretic damper. Earthquake Eng Struct Dyn 1998;27:577–88.

[6] Clark PW, Aiken ID, Tajirian FF, Kasai K, Ko E, Kimura I. Design procedures for buildings incorporating hysteretic damping devices. International Post-SmiRT Conference Seminar on Seismic Isolation, Passive Energy Dissipation and Active Control of Vibrations of Structures, Cheju, South Korea; 1999.

[7] AIK. Design code and commentary for steel structures. The Architectural Institute of Korea, Korea; 1991.

[8] MIDAS/Gen Program. MIDAS/Gen-General structure design system. MIDAS/Gen Ver.5.7.1 Analysis and Design Manual, MIDAS Information Technology, Co., Ltd., http://www.midasit.com.

[9] Tsai KC, Li JW. DRAIN2D+ a general purpose computer program for static and dynamic analyses of inelastic 2D structures supplemented with a graphic processor. Report No. CEER/R86-07, National Taiwan University, Taiwan; 1997.

[10] FEMA. NEHRP Guidelines for the seismic rehabilitation of buildings. FEMA-273 and 274. Washington, DC: Federal Emergency Management Agency; 1997.

[11] Valles RE, Reinhorn AM, Kunnath SK, Li C, Madan A. IDARC 2D version 4.0: a computer program for the inelastic damage analysis of buildings. Technical Report NCEER-96-0010, NCEER, SUNY at Buffalo, 1996.

[12] ATC. Seismic evaluation and retrofit of concrete buildings. ATC-40, Applied Technology Council, Redwood City, California, 1996.

[13] Vanmarcke EH, Gasparini DA. A program for artificial motion generation, user's manual and documentation. Department of Civil Engineering, Massachusetts Institute of Technology; 1976.

[14] SEAOC. Tentative guidelines for performance-based seismic engineering, SEAOC Blue Book. Structural Engineers Association of California; 1999.